Axisymmetric Drop Penetration Into an Open Straight Capillary

Poorya A. Ferdowsi and Markus Bussmann

Department of Mechanical and Industrial Engineering
University of Toronto

Email: *p.ferdowsi@utoronto.ca, bussmann@mie.utoronto.ca*

ABSTRACT

We consider the imbibition of a drop into an open straight capillary. The drop size compared to the hole size, the equilibrium contact angle, and the geometry of the capillary determine whether the drop will draw into the capillary, or not wet the capillary at all. We have developed a numerical scheme based on the Volume of Fluid (VoF) method to study this phenomena. Here we focus on the numerical scheme to treat the contact line motion near a sharp corner, and then present a few results of the dynamics of wetting and dewetting.

1 INTRODUCTION

Contact line-driven flows on rough and porous surfaces occur in a variety of applications, including inkjet printing, enhanced oil recovery, water repellent fabric and self-cleaning surface design, and spray coating. Here we consider a drop atop an open single pore on such a surface, and examine the wetting and dewetting of the capillary. This fundamental analysis sheds light on more complex phenomena such as the wetting and drying of a real fabric surface, structured surface, or porous media.

As shown in figure 1, one can infer three interfacial flow regimes: the flow over the surface around the capillary, the imbibition of liquid into the capillary, and the flow near the sharp corner. While the modelling of contact line flows over flat surfaces (as in regions 1 and 2 in figure 1) remains a topic of research, the focus here is on the development of a methodology for the contact line motion and the dramatic interface deformation near the sharp corner (region 3 in figure 1). We have developed that methodology for the well-known Volume of Fluid (VoF) method, and then used it to simulate the imbibition of a drop into a capillary.

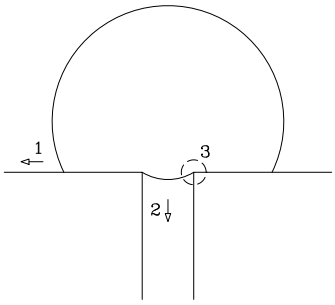

Figure 1: Interfacial flow regimes over and within a capillary: (1) The interface motion on top of the surface, (2) the interfacial flow within the capillary, and (3) contact line pinning and interface deformation near a sharp edge.

The VoF method is a popular choice for tracking interfaces because it can conserve mass exactly [14, 15]. In the VoF method applied to a two-phase flow, the volume fraction f is defined as the ratio of the volume of one (reference) fluid inside a cell to the cell volume. $f = 1$ indicates a full cell while $f = 0$ indicates no reference fluid in the cell. Interface cells are those with $0 < f < 1$; in such cells, the interface is geometrically reconstructed based on f. The most common technique is the Piecewise Linear Interface Calculation (PLIC) method (e.g. [2, 12, 14, 15]) in which the interface is represented by a linear segment within each interface cell. PLIC requires a normal and an intercept for reconstructing the interface within a cell. The intercept can be computed either analytically or iteratively [17], while many methods have been suggested to compute normals (e.g. [6, 12, 13, 14, 15, 18]). In addition to reconstruction, for flow problems that involve surface tension, the mean curvature must be calculated from the volume fractions (e.g. [3, 5]). Finally,

in a two-phase flow simulation, f must be advected in a way that maintains a sharp interface. Algebraic methods are often diffusive; thus the interface is usually advected geometrically (e.g. [14, 16, 18]). By reconstructing and advecting f, the new location of an interface is determined.

Much research has been conducted on the wetting and dewetting of a capillary [4, 8, 9, 10, 19, 20]. Middleman [10] reviews analytical work on liquid imbibition into a capillary, also known as capillary wicking, and penetration dynamics. When a capillary tube comes in contact with an infinite reservoir, the instantaneous capillary rise and wicking speed can be predicted by the Washburn-Rideal-Lucas equation (WRL) [19]. More closely related to the results presented here, Marmur [9] studied the penetration of a single drop, i.e. a finite amount of liquid, into a capillary, assuming that the drop is initially pinned to the tube entrance and that gravity does not distort the drop from a spherical shape. Marmur determined that there is a critical value of the contact angle which distinguishes between penetration and nonpenetration, that depends on the drop size, and can be much greater than 90°. Also, the smaller the drop, the faster it seeps into the capillary.

We have developed a VoF-based methodology for the behaviour of a contact line near a sharp corner, based on the concept of contact line pinning. Here we present details of that methodology, and then some results of capillary wetting and dewetting to illustrate its efficacy.

2 NUMERICAL TREATMENT OF CONTACT LINE MOTION NEAR A SHARP CORNER

Consider the configurations shown in figure 2, of a contact line traversing a solid surface at a corner. At the micro scale shown in figure 2(a), the corner is not sharp, and the contact angle θ is always the actual angle between the tangent line to the solid surface and the interface. However, at the macro level, the corner appears sharp, and we observe different "edge" contact angles θ_{ed} (e.g. $\theta+\alpha_1$, $\theta+\alpha_2$, $\theta+\alpha_3$) that depend on the position of the contact line on the solid at the micro level. According to Gibbs [7, 11], at equilibrium, the edge contact angle θ_{ed} must lie between the contact angles on either side of the corner.

Now consider that the contact line is moving slowly toward a sharp corner. At the micro level, shown in figure 2(a), the contact angle remains constant as the contact line traverses the corner. The distance traveled by the interface is proportional to the radius of curva-

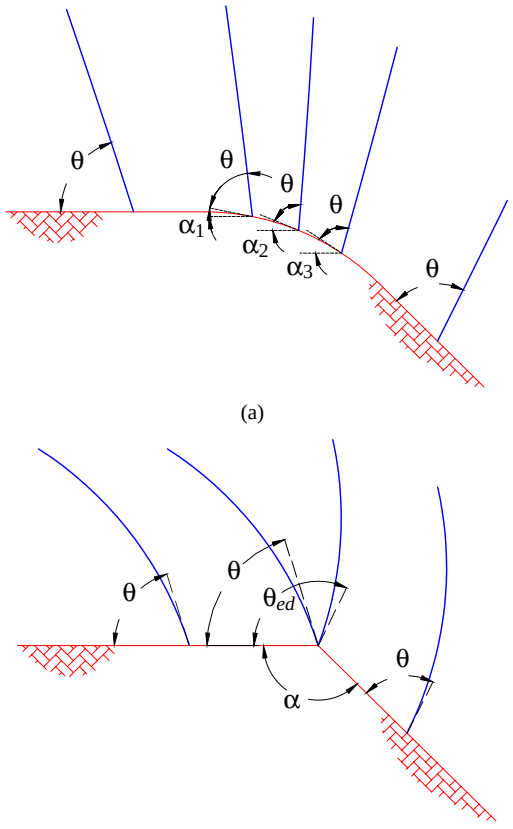

Figure 2: Contact line motion near a corner at (a) the micro scale and (b) the macro scale.

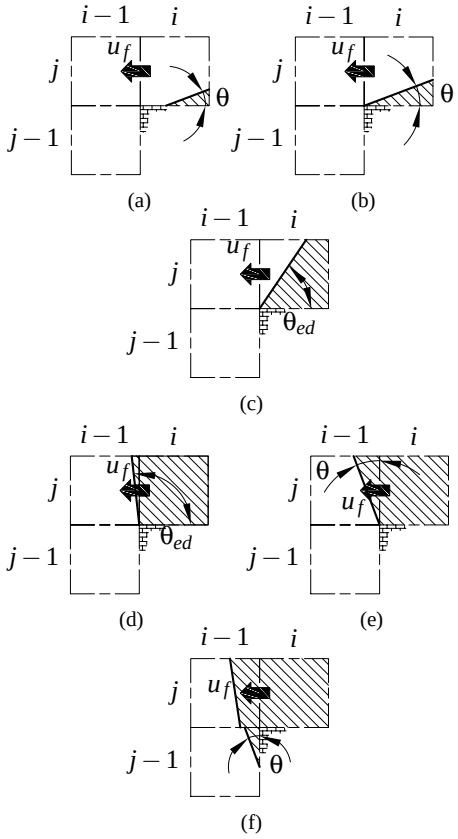

Figure 3: Interface configurations near a sharp corner, when the flow direction is CCW about the corner. Cases (b) and (e) are two special cases, when $\theta_{ed} = \theta$; in practice, an interface configuration will likely change from (a) to (c) (similarly from (d) to (f)) from one timestep to the next.

ture of the corner. As the curvature increases, the distance approaches zero. At the macro scale, the radius of curvature of the corner is negligible compared to any other characteristic dimension, e.g. a drop radius, and so the distance travelled by the contact line can be assumed to be zero. Therefore, at the macro level, when the contact line reaches an ideally sharp corner, it can be assumed to pin there and rotate about the corner, until θ_{ed} reaches the contact angle associated with the other side, as illustrated in figure 2(b).

A VoF treatment of a contact line at a sharp corner requires modification of both the interface reconstruction algorithm (i.e. the computation of θ_{ed}) and the advection scheme. For the sake of simplicity, we assume that $\theta < \dfrac{\pi}{2}$.

Consider that a liquid moves counter clockwise about a corner, and that the contact line approaches the sharp corner from the right, as depicted in figure 3(a). When the contact line reaches the corner (figure 3(b)), it pins there. The volume fraction in the cell (i, j) at this instant, f_p, can be calculated from simple geometry. Hereafter, the edge contact angle starts increasing as more liquid enters the cell (i, j) (figure 3(c)), so that $f_{i,j} > f_p$. Since the contact line is pinned, only the gas phase can be allowed to pass across the left face of the cell (i, j), until $f_{i,j} = 1$. $\theta_{ed}^{i,j}$ can be computed based on $f_{i,j}$. Thereafter, the contact line remains pinned until $\theta_{ed}^{i-1,j} = \theta + \pi/2$ (figure 3(e)) during which time only the gas phase can be allowed to pass across the bottom face of the cell $(i-1, j)$, until the contact line releases (figure 3(f)). From this description, it can be inferred that two VoF modifications are required: to calculate $\theta_{ed}^{i,j}$ based on $f_{i,j}$ (reconstruction step), and to modify the advection scheme so that only one of the phases advects across nearby cell faces when the contact line is pinned.

These modifications were applied to the height function (HF) technique for calculating interface normals and curvatures [1, 3], and to the EI-LE advection technique of Scardovelli and Zaleski [18]. Details will be presented in a subsequent paper.

3 RESULTS

We now present the results of two simulations, one for a wetting contact angle of 60°, and the other for a non-wetting angle of 120°. In both cases, we initially place a drop partially within a capillary in the axisymmetric coordinate system. The drop is assigned the properties of water; the surrounding gas is air.

For the first case presented here, the radius of the drop is 15 μm, the radius of the capillary is 18.75 μm and the initial penetration depth is 17 μm. Based on these parameters the Ohnesorge number, that here reflects the ratio of viscous to surface tension forces, is $\mathbf{Oh} = 0.034$.

We investigate the problem by introducing two parameters. Denoting the velocity vector in cell (i, j) by $\vec{V}_{ij} = (u_{ij}, v_{ij})$, the average seeping velocity $\bar{v_s}$ of fluid within the capillary is:

$$\bar{v_s} = \frac{\sum_{\text{in hole}} f_{ij}\Omega_{ij} \cdot v_{ij}}{\sum_{\text{in hole}} f_{ij}\Omega_{ij}} \qquad (1)$$

where Ω_{ij} is the 3D axisymmetric volume of the cell (i, j). When there is no liquid in the capillary, $\bar{v_s} = 0$. The second parameter reflects the centroid of the fluid

in the z direction, which is computed as:

$$z_m = \frac{\sum_{\text{all cells}} f_{ij}\Omega_{ij}z_{ij}}{\sum_{\text{all cells}} f_{ij}\Omega_{ij}} \qquad (2)$$

Figure 4 shows the position of the imbibed drop at 10 μs increments; figure 5 shows close-ups of the contact line while pinned at the corner. (Note that for all results presented here, the interfaces are the actual piecewise linear segments from the VoF PLIC reconstruction, and not simply a contour plot of $f = 1/2$.) The variation of $\bar{v}_s$ versus time is plotted in figure 6, and z_m in figure 7.

As shown in figure 4(a), the drop is initially positioned partially within the capillary, but immediately begins to be imbibed by the capillary. Sometime between 7.5 and 8 μs the upper contact line reaches the edge of the capillary opening and is pinned at the sharp edge. The instant when the interface is pinned corresponds to the maximum seeping velocity $|\bar{v}_s|$ shown in figure 6, which reflects that the drop accelerates from $t = 0$ until it reaches the sharp corner. The pinning duration, i.e. the time that the upper meniscus remains pinned, is about 3 μs. It is during this interval that the edge contact angle changes from that associated with the top surface to that associated with the capillary, as fluid rapidly enters the capillary. Due to the high velocity as well as the continuous change in the edge contact angle, the upper meniscus deforms dramatically during those 3 μs. After $t \approx 9.5$ μs, no liquid remains above the capillary. After the release of the contact line from the sharp corner, sometime between 11 and 11.5 μs, viscous damping and the surface tension force decelerate the column of fluid sliding into the capillary. The asymptotic behavior of z_m shown in figures 6 and 7 illustrates that by $t \approx 100$ μs the column of liquid has reached equilibrium ($z_m \approx 78$ μm). At $t = 100$ μs, $h = 18.293$ μm is the penetration depth measured from the top solid surface.

Now consider the non-wetting case, when the contact angle is 120°. Figure 8 shows the position of the drop in 25 μs increments. The variation of $\bar{v}_s$ with time is shown in figure 9, and z_m is plotted in figure 10.

Figure 8(a) shows the drop initially positioned partially within the capillary, similar to the previous case. The exact equilibrium configuration, based on a thermodynamic analysis presented elsewhere, is indicated by the dashed line; at $t > 0$, liquid begins to rise. Around 240 μs the interface reaches the edge of the capillary opening. This is the time when z_m and $\bar{v}_s$ manifest oscillations due to the pinning effect. Note

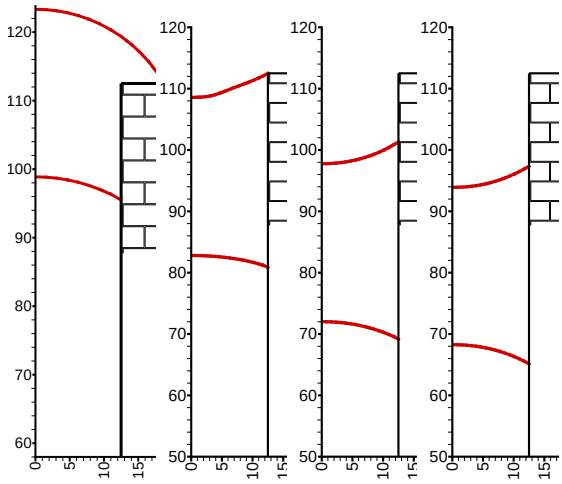

(a) 0 μs (b) 10 μs (c) 20 μs (d) 30 μs

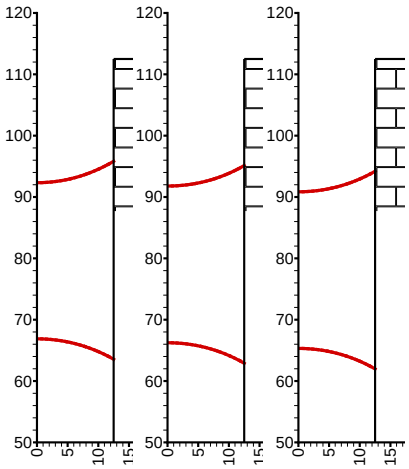

(e) 40 μs (f) 50 μs (g) 100 μs

Figure 4: Case I, $\theta = 60°$: drop imbibition into a capillary. By $t = 100$ μs the fluid has almost reached equilibrium. The dimensions are in μm.

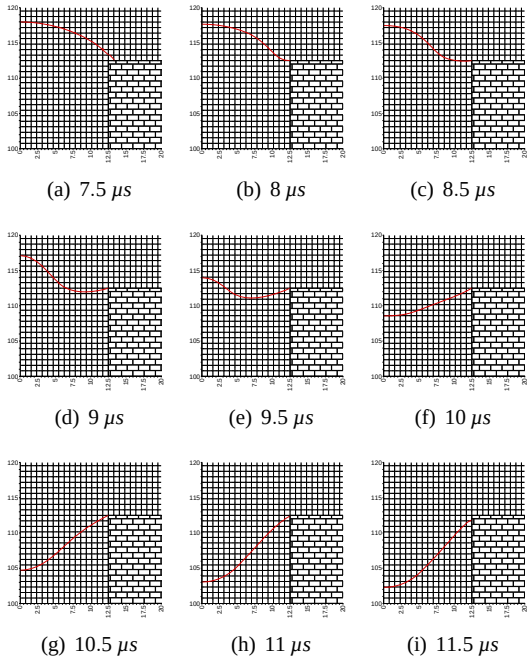

(a) 7.5 μs (b) 8 μs (c) 8.5 μs

(d) 9 μs (e) 9.5 μs (f) 10 μs

(g) 10.5 μs (h) 11 μs (i) 11.5 μs

Figure 5: Case I, $\theta = 60°$: contact line transition from slipping to pinned and again slipping (releasing) near a sharp corner. The dimensions are in μm.

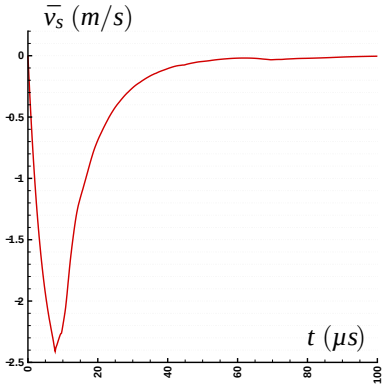

Figure 6: Case I, $\theta = 60°$: variation of the seeping velocity versus time.

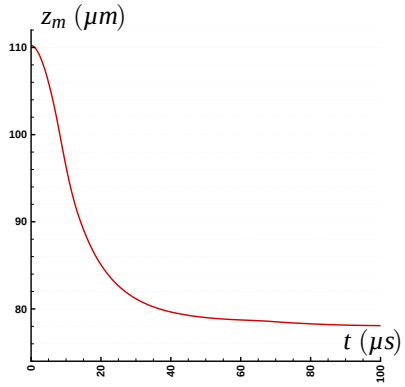

Figure 7: Case I, $\theta = 60°$: liquid position versus time.

that in this case due to the initial amount of liquid within the capillary, the velocity of the lower meniscus, when it reaches the sharp corner for the first time, is not enough to force the release of the pinned contact line from the corner. There can be cases that depend on the initial configuration, when the velocity of the lower meniscus is enough to force the release of the contact line from the edge, only to pin again to the edge and to oscillate between these states, until equilibrium is reached. Although the contact line is pinned, because of the inertia of the moving liquid, the viscous and surface tension forces cannot immediately arrest the motion at the instant of first pinning. As a result the liquid moves slightly upward until the resultant force that acts in the opposite direction stops the liquid at $t = 237$ μs (the first time when $\bar{v}_s = 0$ on figure 9).

Since the resultant force is not zero, the liquid accelerates back into the capillary and θ_{ed} decreases. Such oscillations are observed until the liquid comes to rest. Even at $t = 400$ μs, the upper interface still vibrates while $\bar{v}_s \approx 0$ (see figure 9), because of the periodic deformations of the upper meniscus with an area much bigger than that of the lower meniscus. The edge contact angle at the end of the simulation is $\theta_{ed}^{(400)} = 115.190°$, which is only 0.28% different than the thermodynamic prediction.

4 Conclusion

We have presented a VoF-based treatment for contact line motion around a sharp corner, involving modifications both to the reconstruction and advection steps, and applied an axisymmetric VoF code to the prediction of drop imbibition into a capillary. Examples of both wetting and non-wetting behaviour illustrate very interesting dynamics of a contact line pinned to the capillary edge.

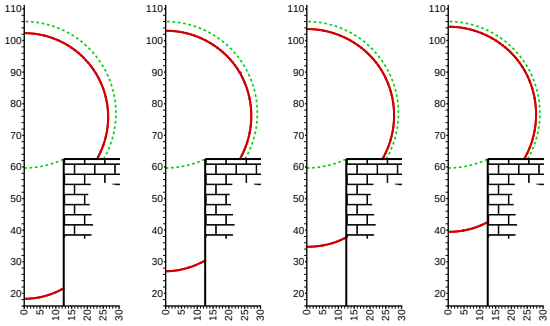

(a) 0 μs (b) 100 μs (c) 150 μs (d) 175 μs

(e) 200 μs (f) 225 μs (g) 250 μs (h) 400 μs

Figure 8: Case II, $\theta = 120°$: the drop pulls out of the capillary. By $t = 400$ μs the bottom meniscus has almost reached equilibrium but the upper interface still oscillates. The dashed line is the exact equilibrium configuration. All dimensions are in μm.

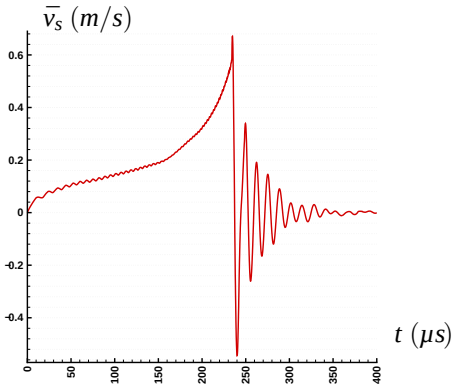

Figure 9: Case II, $\theta = 120°$: variation of the seeping velocity versus time.

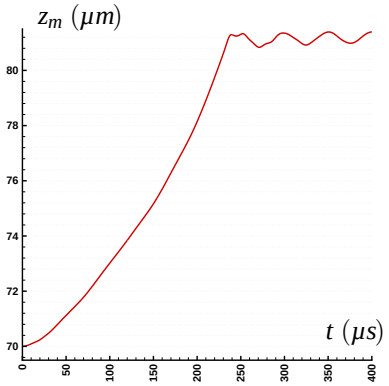

Figure 10: Case II, $\theta = 120°$: liquid position versus time.

REFERENCES

[1] S. Afkhami and M. Bussmann. Height functions for applying contact angles to 2D VOF simulations. *International Journal for Numerical Methods in Fluids*, 57(4):453–472, 2008.

[2] N. Ashgriz and J. Y. Poo. FLAIR: Flux line-segment model for advection and interface reconstruction. *Journal of Computational Physics*, 93(2):449–468, 1991.

[3] S. J. Cummins, M. M. Francois, and D. B. Kothe. Estimating curvature from volume fractions. *Computers and Structures*, 83(6-7):425–434, 2005.

[4] A. Delbos, E. Lorenceau, and O. Pitois. Forced impregnation of a capillary tube with drop impact. *Journal of Colloid and Interface Science*, 341(1):171–177, 2010.

[5] M. M. Francois, S. J. Cummins, E. D. Dendy, D. B. Kothe, J. M. Sicilian, and M. W. Williams. A balanced-force algorithm for continuous and sharp interfacial surface tension models within a volume tracking framework. *Journal of Computational Physics*, 213(1):141–173, 2006.

[6] S. H. Garrioch and B. R. Baliga. A PLIC volume tracking method for the simulation of two-fluid flows. *International Journal for Numerical Methods in Fluids*, 52(10):1093–1134, 2006.

[7] J. W. Gibbs. The scientific papers. *Il Nuovo Cimento Series 5*, 15(1):526–528, 1908.

[8] E. Lorenceau and D. Quere. Drops impacting a sieve. *Journal of Colloid and Interface Science*, 263(1):244–249, 2003.

[9] A. Marmur. Penetration of a small drop into a capillary. *Journal of Colloid and Interface Science*, 122(1):209–219, 1988.

[10] S. Middleman. *Modeling Axisymmetric Flows : Dynamics of Films, Jets, and Drops*. Academic Press, San Diego, 1995.

[11] J. F. Oliver, C. Huh, and S. G. Mason. Resistance to spreading of liquids by sharp edges. *Journal of Colloid and Interface Science*, 59(3):568–581, 1977.

[12] B. Parker and D. Youngs. Two and three dimensional Eulerian simulation of fluid flow with material interfaces. *UK Atomic Weapons Establishment*, 01/92, 1992.

[13] J. E. Pilliod Jr. and E. G. Puckett. Second-order accurate volume-of-fluid algorithms for tracking material interfaces. *Journal of Computational Physics*, 199(2):465–502, 2004.

[14] W. J. Rider and D. B. Kothe. Reconstructing volume tracking. *Journal of Computational Physics*, 141(2):112–152, 1998.

[15] M. Rudman. Volume-tracking methods for interfacial flow calculations. *International Journal for Numerical Methods in Fluids*, 24(7):671–691, 1997.

[16] R. Scardovelli and S. Zaleski. Direct numerical simulation of free-surface and interfacial flow. *Annual Review of Fluid Mechanics*, 31:567–603, 1999.

[17] R. Scardovelli and S. Zaleski. Analytical relations connecting linear interfaces and volume fractions in rectangular grids. *Journal of Computational Physics*, 164(1):228–237, 2000.

[18] R. Scardovelli and S. Zaleski. Interface reconstruction with least-square fit and split Eulerian-Lagrangian advection. *International Journal for Numerical Methods in Fluids*, 41(3):251–274, 2003.

[19] E. W. Washburn. The dynamics of capillary flow. *Physical Review*, 17(3):273–283, 1921.

[20] G. R. Willmott, C. Neto, and S. C. Hendy. An experimental study of interactions between droplets and a nonwetting microfluidic capillary. *Faraday Discussions*, 146:233–245, 2010.